Incommensurate phases in barium sodium niobate: Transmission-electron-microscopy study

S. Barre, H. Mutka,* and C. Roucau
Laboratoire d'Optique Electronique du Centre National de la Recherche Scientifique, Boite Postale 4347, 31055 Toulouse Cedex, France
(Received 22 February 1988)

A transmission-electron-microscopy study of barium sodium niobate has confirmed new features of the incommensurate phase. We present here images showing the nucleation of the incommensurate phase when the temperature increases after thermal cycling the sample or annealing in the incommensurate phase. In agreement with previous inferences, *in situ* annealing either at 230 °C near the lock-in transition or at 270 °C close to the tetragonal normal phase transition can favor the stability of a unidirectional $1q$ or a doubly modulated $2q$ incommensurate phase, respectively. The difference in the orientation of discommensurations, either perpendicular to the orthorhombic a axis or perpendicular to the tetragonal a and b axes, agree with an assignment of the two phases based on theoretical arguments and on x-ray and optical data.

I. INTRODUCTION

The incommensurate phase (IP) of barium sodium niobate (BSN) has been widely studied by means of x-ray diffraction,[1] neutron scattering,[2] and birefringence.[3] It presents particular properties such as hysteresis, relaxation, and memory effects,[4] which were originally attributed to the interaction of the incommensurate modulation with defects existing in the sample. Based on x-ray goniometric and precession measurements, as well as on optical data and Landau theoretical considerations, it has recently been shown[5–9] that another interpretation was in order. The temperature range previously assigned to a single IP is actually occupied by two IP's. One is the orthorhombic IP, modulated along a single direction and previously considered alone. It is stable in the lower range of temperatures, nearby the lock-in transition, and is metastable above this range. The other is a tetragonal IP modulated along two perpendicular directions, and stable in the upper temperature range nearby the normal-incommensurate transition, and metastable below this range. Between the two ranges, a phase transition has been assumed to exist which connects the two IP's. This complex situation is sketched in Fig. 1. In this framework, the source of the thermal hysteresis has been assigned essentially to the metastability of the IP.

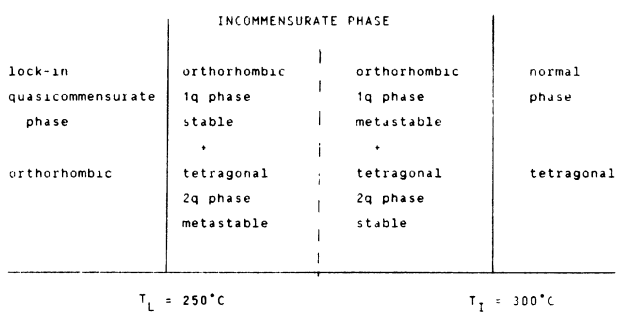

FIG. 1. Phase diagram of BSN from room temperature to 580 °C.

Indirect support only has been obtained for this interpretation from a previous transmission-electron-microscopy (TEM) study, revealing that one can quench, at room temperature, the boundaries between two phases.[6] However, up to now, no direct observation of the two phases could be performed within their range of stability. Such an observation was hampered, on the one hand, by the weakness of the reflections which can be used to build the images, and, on the other hand, by the complexity of the pictures obtained whenever the two IP's coexist.

In this paper, we show, for the first time, direct evidence of the occurrence of the two IP's. In this view, we have used the memory effect specific to incommensurate systems[6,10] in order to destabilize one of the IP's and isolate the other in the temperature range of the IP. Other important features of our measurements are to show the kinetics of the transition between the commensurate phase and the incommensurate one, either in the absence of any special preparation of the samples, or in the case where one of the IP's has been destabilized, to point out the role of preexisting walls [ferroelastic domain boundaries and discommensurations (DC's)] in the nucleation process of new discommensurations, and to show clear evidence of pinning of the DC by defects of the structure.

II. EXPERIMENTAL DETAILS

Single crystals of BSN were grown using the Czochralski method by Joukoff and Aubrée at Centre National d'Etudes des Télécommunications (CNET) Bagneux. Their measured composition in oxide contents was 8.08 mol% Na_2O, 41.57 mol% BaO, and 50.35 mol% Nb_2O_5. (001) plates were polished, mechanically, down to a thickness of about 50 μm and then thinned by ion-beam milling. The specimens were observed in a JEM 200 CX electron microscope coupled with a video camera. *In situ* observations at high temperature were undertaken with the Jeol specimen heating holder. Temper-

ature was controlled by a programmable temperature regulator. Images were obtained by the dark field method, selecting incommensurate satellite reflections strongly excited by tilting the sample slightly from the [001] zone axis. As the temperature increased, the satellite intensity decreased, so the quality of the images at high temperature was not as good as the one obtained at room temperature. Moreover, the specimen single tilt holder did not allow a perfect orientation of the sample.

The absence of contact between the thermocouple and the sample, as well as the local heating produced by the electron beam, led to a temperature measurement slightly different from the exact temperature of the observed zone. The difference may depend on samples due to the different thermal contact of the thin part. Comparison with diffraction results obtained with x rays or neutrons shows that the difference is less than 10 K for a good thermal contact of the TEM sample. As the range of stability of the IP of BSN depends strongly on the thermal history of the sample, all experiments as a function of temperature were performed at the heating or cooling rate of 2.5 °C/min between 20 °C and 350 °C, which is the reference rate used by Schneck *et al.* in their experiments.[11] For fast-cooling experiments, samples were quenched down in a few minutes by switching off the furnace power supply. In order to minimize irradiation damage[12] which can affect the transitions temperatures even for experiments at 200 kV, we irradiated the sample just for the time necessary to take a photograph.

III. EXPERIMENTAL RESULTS

A. Behavior of BSN during thermal cycling

In this paragraph, we first describe the quasicommensurate phase observed at room temperature (RT), then examine the thermal variation of the incommensurability parameter δ measured on the electron diffraction pattern. The evolution of the DC pattern when the temperature increases, as recorded on a video tape, is outlined, and micrographs of the IP obtained at 230 °C are analyzed.

1. Room-temperature observations

At RT, diffraction studies[1,2] show that satellite reflections deviate by about $\delta \approx 1\%$ from the commensurate value; the stable phase is "quasicommensurate." This result is consistent with the presence of dark wavy lines observed on satellite micrographs, which have been reliably identified with the DC's (Refs. 13, 14, and 15). Indeed, the density of these lines is proportional to δ and a microdiffraction observation between these lines reveals a perfect commensurate state. Each DC corresponds to a phase shift of $\pi/2$ of the modulation and they join together in fourfold nodes. A typical view of the quasicommensurate phase is presented in Fig. 2. We observe two ferroelastic domains separated by a ferroelastic wall having the $[100]_t$ orientation. The two variants differ by the direction of modulation: The a_0 and b_0 axis are interchanged in the two domains. The DC pattern is composed of dark wavy lines which follow the $[110]_t$ direction, on the average, at 45° from the ferroelastic wall.

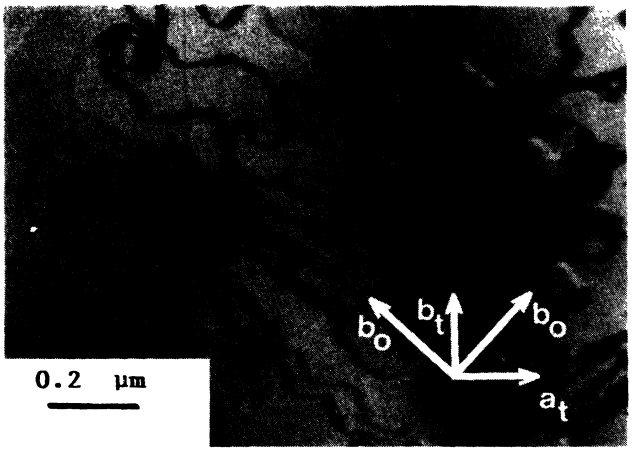

FIG. 2. Satellite dark-field micrograph obtained at RT. Two ferroelastic variants separated by a ferroelastic wall parallel to a_t or b_t are visible. In each domain, dark lines, parallel to b_0, on the average are discommensurations.

The DC pattern observed at RT depends on the thermal processing of the sample, especially on prolonged annealing within the IP (Ref. 6). In a general case, the DC pattern is rather disordered. This absence of a good ordering in the DC orientation can be thought to be due to a pinning by point defects of the structure. This is confirmed by the fact that the pattern observed at RT before and after a cycle are precisely superposable: the DC's recover their exact position and shape. This observation is illustrated in Fig. 3. The micrograph was taken at the end of a cycle on the same region as the one presented in Fig. 2.

2. Thermal variation of the wave vector

The evolution with temperature has been studied both in direct and reciprocal space. The evolution of the incommensurability parameter δ, measured on an electron diffraction pattern when the sample is cycled from RT to 350 °C at the constant rate of 2.5 °C/min, is presented in

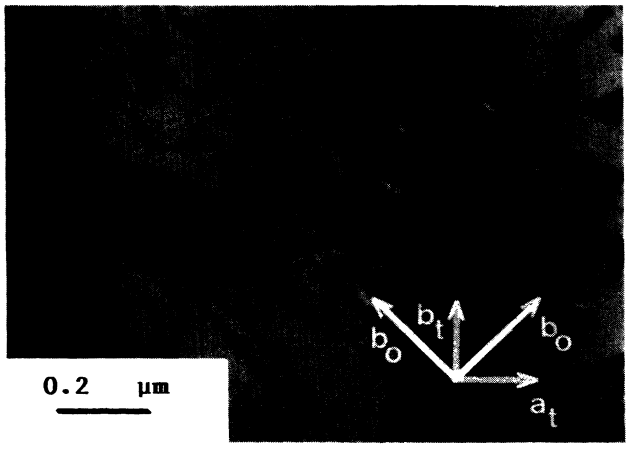

FIG. 3. Satellite dark-field micrograph obtained at RT at the end of a cycle on the same region as the one presented in Fig. 2. We observe the same pattern of DC.

Fig. 4: From RT to T_L, δ is constant, but nonzero in the quasicommensurate phase; at T_L we can note a discontinuity in the value of δ, then it varies linearly between 0.08 at T_L and 0.12 at T_I. A strong hysteresis is recorded on cooling until δ reaches the value it had at the beginning of the cycle. Our results are in good agreement with those obtained from x-ray precession experiments[1] and elastic neutron scattering experiments.[2] We have observed that long exposures under the electron beam affect, very significantly, the variation of δ. This effect denotes the influence of irradiation defects. We have studied it in detail by performing calibrated irradiations inside or outside of the microscope. The corresponding results will be reported separately.[7]

3. *Nucleation of the INCP in a nonannealed sample*

With the camera video coupled wit the microscope, we have followed the evolution of the DC pattern from RT to the normal phase. This evolution is presented on the series of micrographs in Fig. 5. Above 200 °C, the density of DC increases rapidly as δ, measured on the diffraction pattern varies. When the temperature is increased at 2.5 °C/min, black points start to appear upon an existing DC or between two DC. Then, these points spread out and form small loops containing four truncated DC's. The loops do not extend because of their high density. Finally, the DC pattern becomes very complex and it is difficult to determine a direction of growth. At this stage of the experiment we measure on the diffraction pattern a δ of about 5%. It is worth pointing out that the DC existing at the beginning of the experiment are unchanged and quite immobile during the heating, probably due to their pinning by defects.

Figure 6 shows a micrograph obtained at 230 °C. We observe a complicated structure composed of grey and white little domains which are a complex texture of the DC's and ferroelastic microdomains. At this scale, we cannot distinguish between ferroelastic walls and DC. We can note that preferred orientations $[100]_t$ and $[010]_t$ start to develop. These are the directions of ferroelastic domain walls, at 45° from the DC in the quasicommensurate phase. On this photograph we have measured the average distance between two walls ($\sim$15 nm). Considering that this distance is the average distance between two DC, we can calculate δ as the incommensurability parameter, and find $\delta \approx 6\%$. This result is in good agree-

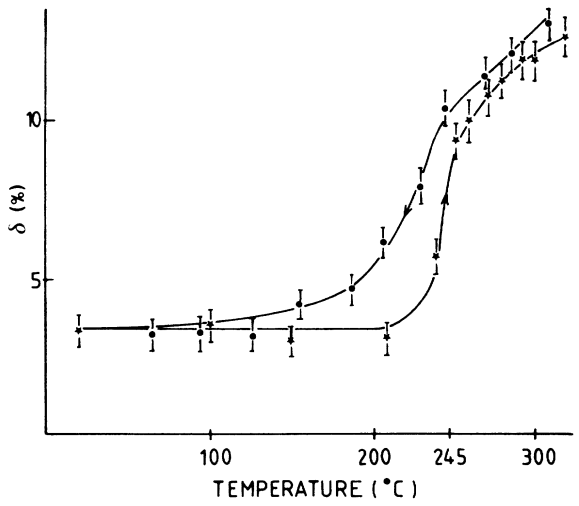

FIG. 4. Thermal variation of the incommensurability parameter δ determined from an electron diffraction experiment during a cycle from RT to the normal phase at 2.5 °C/min. $T_L = 245$ °C is the temperature of the lock-in transition, and $T_I = 310$ °C is the temperature of the IP→normal phase transition.

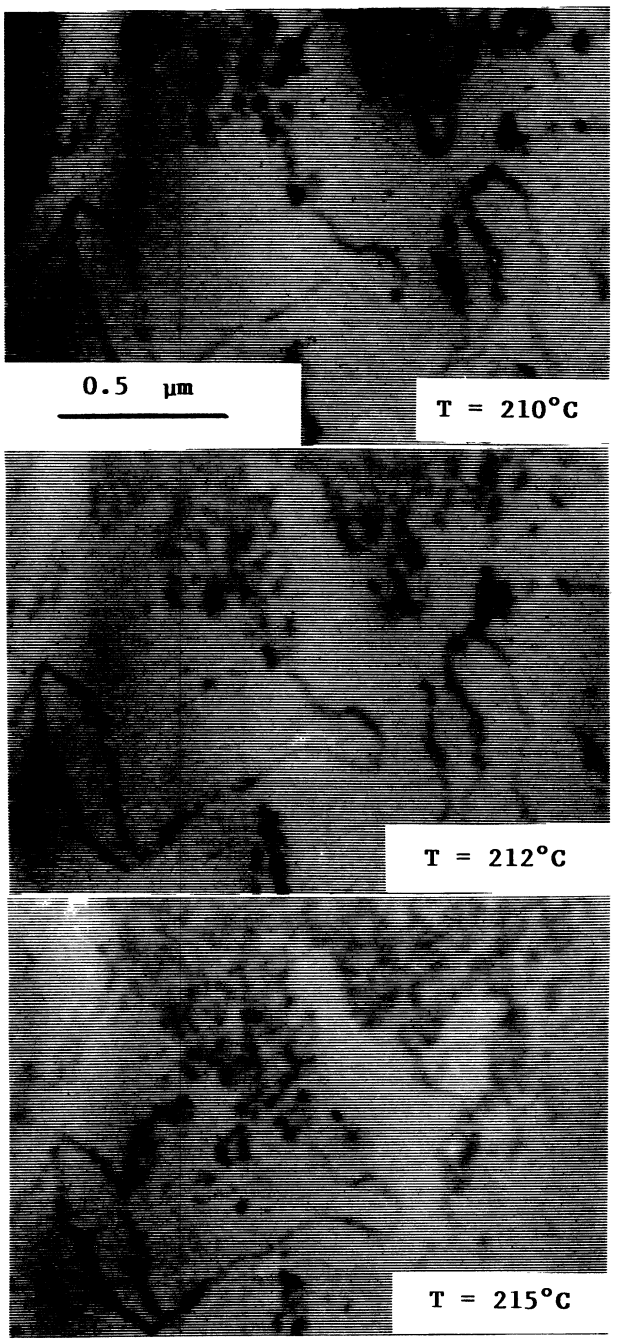

FIG. 5. This sequence shows the development of the incommensurate phase during a heating run at 2.5 °C/min. It occurs by nucleation of the discommensurations.

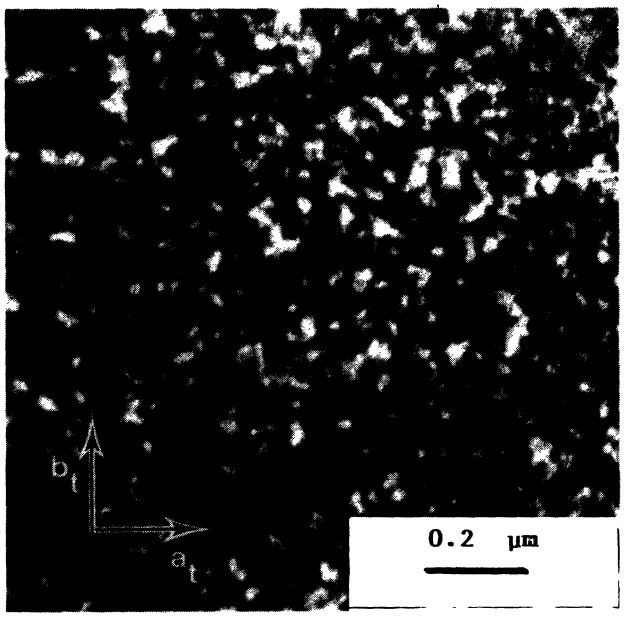

FIG. 6. Satellite dark-field micrograph of the incommensurate phase obtained at $T=230\,°C$.

ment with the measurement of $\delta \approx 6\%$ on the electron diffraction pattern.

In line with the preceding observations, we have performed a diffraction study on a single ferroelastic domain region of the sample. At RT, diffraction from one domain exhibits one direction of modulation; the wave vector is parallel to the a_0 axis. When the temperature increases, diffuse streaks appear around positions turned by 90° from the satellite positions. These streaks finally condense into spots which correspond to a direction of modulation perpendicular to the first one. At high temperature, the diffraction pattern resembles the diffraction pattern of a multidomain ferroelastic region. At 290 °C, the intensities of the two variants are equivalent and we can measure $\delta_1=\delta_2\approx 12\%$. When we come back to RT, we again observe one direction of modulation only.

A natural explanation is to consider a multiplication of ferroelastic microdomains of the modulated orthorhombic phase ($1q$ phase). On the assumption of the presence of a mixing of two modulated phases ($1q$ phase and $2q$ phase) (Refs. 6–8), our results suggest that it can be a nucleation of a tetragonal phase with two perpendicular directions of modulation ($2q$ phase) in the modulated orthorhombic phase ($1q$ phase). In any case, such complicated images do not permit us to conclude and determine the structure of the two phases. New experiments were then performed showing that two distinct growth processes of the IP could be obtained after an appropriate annealing. They are described in the following paragraph.

B. Behavior of BSN after annealing in the IP

In this section we describe the results obtained through an experimental procedure which uses the memory effect known to exist in BSN from x-ray and birefringence measurements.[5,11]

This effect appears during the heating run following an annealing at T_A within the IP and a subsequent quench at RT. We present here the pecularities of the nucleation of the IP in the conditions of thermal processing which induces a memory effect. The microstructure obtained at RT after the quench depends on the nature of the IP at T_A, i.e., on the mixing of the phases $1q$ and $2q$ and on their respective interaction with defects. Previous TEM investigation at RT showed evidence for the presence of two types of regions in the crystal differing by the spatial distribution of the DC (Ref. 6).

(a) Regions with a very low density of DC which do not possess the expected $[110]_t$ orientation but with the direction perpendicular to the ferroelastic wall.

(b) Regions with a high density of DC lying in the $[110]_t$ direction. Their density depends on the annealing temperature.

We have annealed the sample at two temperatures, chosen considering the phase diagram presented in the Introduction:

(a) At $T_A=230\,°C$, slightly below the lock-in temperature, where the orthorhombic phase is stable.

(b) At $T_A=270\,°C$, in the IP where the modulated tetragonal phase is stable.

We have chosen to follow the nucleation in a low-density region of DC so the new phase can develop easily without interfering with other DC's. After this treatment, we discover two quite distinct processes of growth of the IP.

(i) Figure 7 shows the nucleation after annealing at $T_A=230\,°C$, which is situated near the lower limit of the IP just above the lock-in transition. At about 220 °C, black lines grow precisely along b_0. We do not observe loops, and rapidly all space is recovered by a quite regular DC pattern consisting of fringes parallel to the b_0 axis. In the adjacent domain, the same phenomenon occurs in the perpendicular direction. These unusual contrasts are observed up to the IP→normal phase transition until the satellite intensity vanishes. These contrasts are not as complicated as those obtained in Fig. 6, and the image closely resembles the pattern of DC observed in other incommensurate compounds, i.e., an array of equally spaced DC's perpendicular to the q vector of the modulation. For instance, the images obtained resemble the incommensurate microstructure of $2H$-$TaSe_2$ (Refs. 16 and 17).

(ii) Figure 8 shows the nucleation after annealing at $T_A=270\,°C$, which is situated in the upper range of the IP. We first note the emergence of black points which do not extend. Then, rapidly, a complicated structure formed by black, grey, and white domains is obtained by a multiplication of the ferroelastic domains, i.e., at 45° of the array observed earlier in (i). At 230 °C, we discover two preferred directions $[100]_t$ and $[010]_t$. When the temperature increases, the intensity of the image decreases and the IP→normal phase transition occurs.

IV. DISCUSSION

Referring to the phase diagram in Fig. 1, conjectured to represent the situation in BSN (Ref. 9), we are able to

interpret the result of experiments (i) and (ii). We interpret the observation in (i) as a stabilization of the $1q$ phase in all the temperature range of the IP, the $2q$ phase being absent. The observation in (ii) corresponds to the opposite situation where the $1q$ phase is absent and the $2q$ phase is stabilized alone. The DC structures of the $1q$

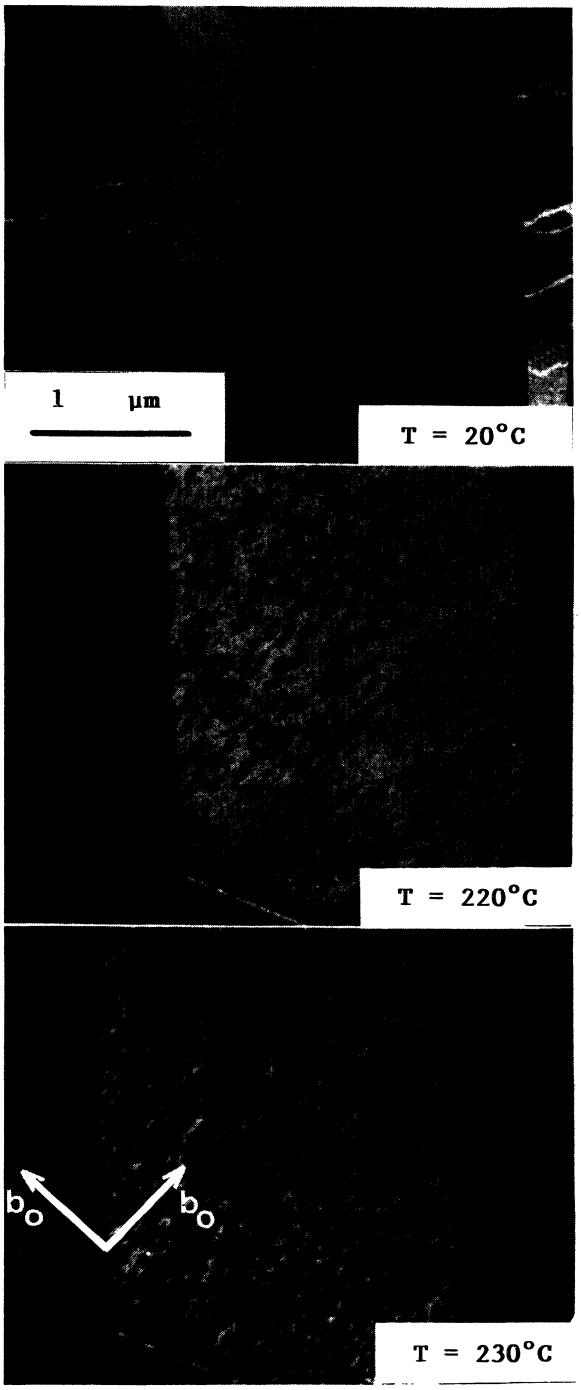

FIG. 7. Satellite dark-field micrographs obtained at different temperatures during a thermal cycle at 2.5 °C/min after annealing at $T_A = 230$ °C. We observe the nucleation of the $1q$ phase in the $[1\bar{1}0]_t$ priviledged direction. In the two neighboring ferroelastic domains the nucleation of the IP occurs in two perpendicular directions.

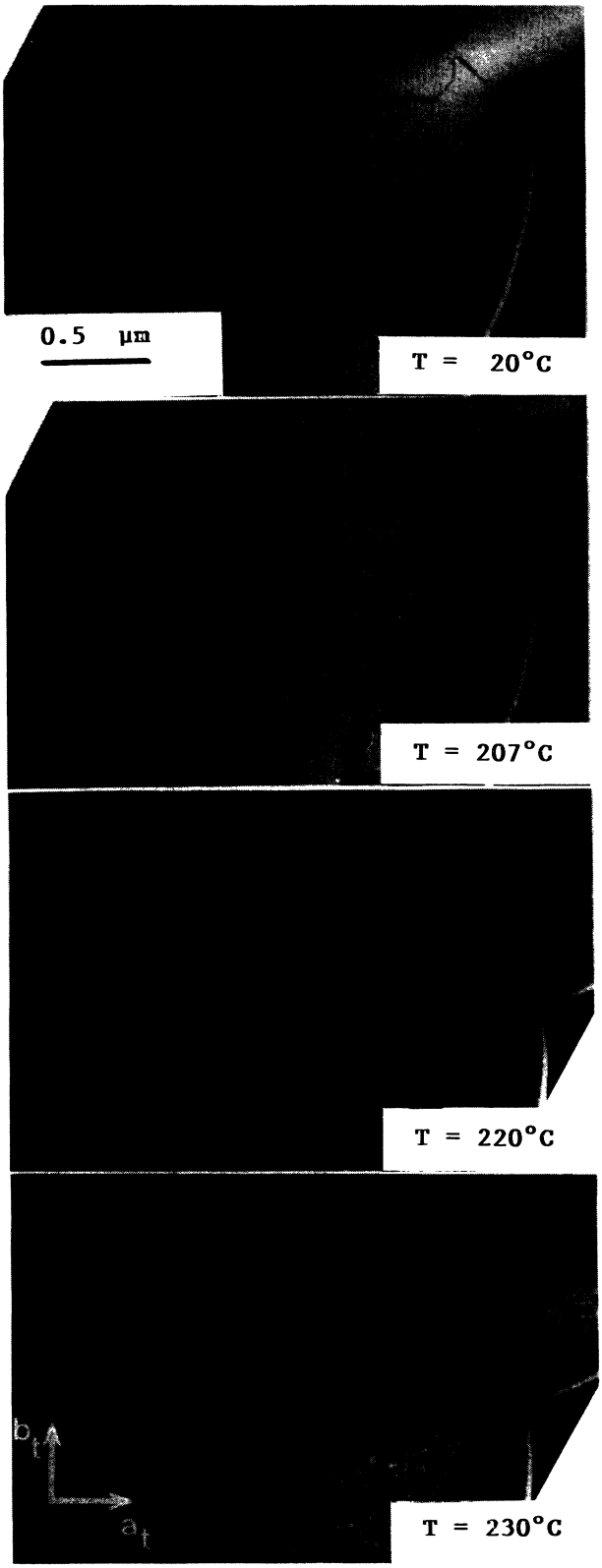

FIG. 8. Satellite dark-field micrographs obtained at different temperatures during a thermal cycle at 2.5 °C/min after annealing at $T_A = 270$ °C. We observe the nucleation of the $2q$ phase by multiplication of ferroelastic domains.

$1q$ and $2q$ phases have been discussed elsewhere.[8] This detailed discussion cannot be entirely repeated here since it relies on complex x-ray and birefringence data as well as theoretical considerations.[18] We restrict ourselves here to a summary of the conclusions which are relevant to our observations.

The domain structure of the $1q$ phase corresponds to the usual domain structure of a singly modulated phase and has been described in the first paragraph concerning the quasicommensurate phase. Eight different domains of the modulation are possible, separated by two types of walls: ferroelastic walls, parallel to the $[100]_t$ or $[010]_t$, and DC walls, parallel to the $[110]_t$ directions (see Fig. 9).

The $2q$ phase has been suggested to be constituted of an ordered array of microscopic ferroelastic domains, i.e., an array of singly modulated regions ordered in two dimensions (see Fig. 10). However, the ordering of the observed pattern is not clear in our pictures. This observation alone cannot consitute evidence of the tetragonal character of this phase and of its unusual arrangement of DC's. Our observation is consistent with the available theoretical picture, and it strengthens the validity of this picture which was partly based on measurements by other techniques (x-ray or optical).

Finally we can also interpret, in the same framework, the more complex pictures obtained during a normal cycling by assigning them to the mixing in various proportions of the two considered phases which coexist in these experimental conditions. Indeed, these pictures do show some features of the $1q$ phase (DC's normal to the $[110]_t$ direction), and some features of the $2q$ phase (small ferroelastic domains).

V. CONCLUSION

In this study we have reported on the thermal variation of electron diffraction patterns and micrographs while it transforms from the lock-in phase to the IP. Periodicity of the images corresponds well to the diffraction results, but we cannot observe clearly defined DC patterns. In spite of this handicap, we conclude that the observed situation is more complex than a single modulated $1q$ phase. In agreement with recent x-ray and optical studies,[8] we assume a phase mixture of the $1q$ and $2q$ phases. This picture is further confirmed by the micrographs obtained after annealing the sample in the respective ranges of the two IP's. Two distinct directions of DC characterize the $1q$ and $2q$ phases, parallel to the b_0 orthorhombic axis or to the a_t and b_t tetragonal axis, respectively.

Qualitatively, these observations of the $1q$ phase and $2q$

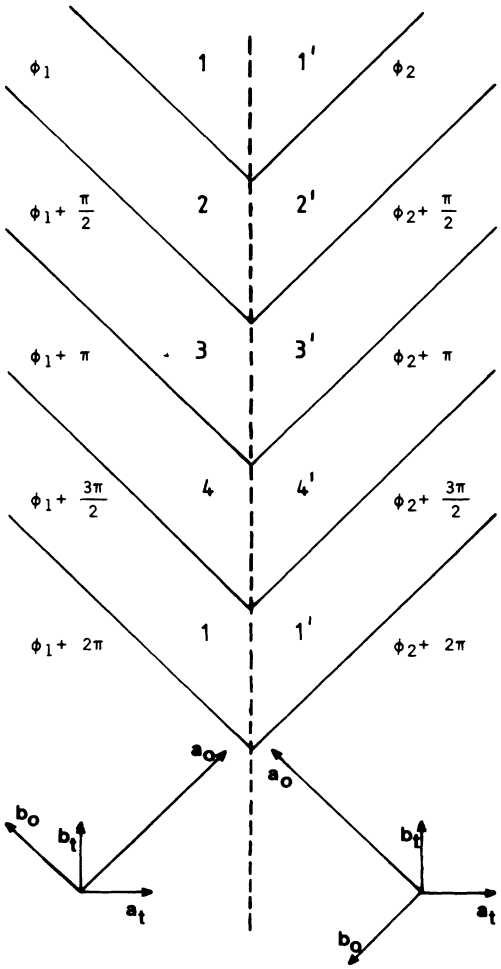

FIG. 9. Perfect domain structure of the $1q$ phase. a_t and b_t (a_0 and b_0) are basic vectors of the tetragonal (orthorhombic) structure. Ferroelastic domains 1 and 2, separated by a dashed line differ by the direction of modulation. DC's (solid lines) correspond to a phase shift of $\pi/2$ of the modulation. So, we can define eight possible states.

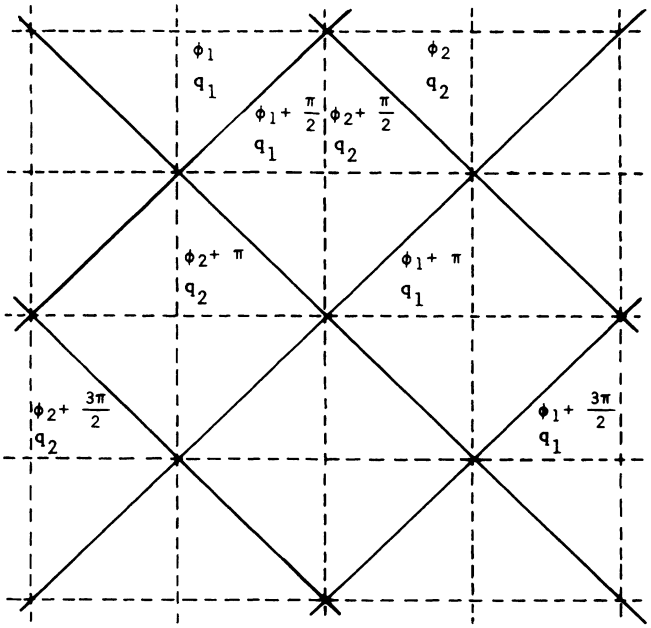

FIG. 10. Perfect domain structure of the $2q$ phase composed of ferroelastic microdomains differing by the direction of modulation. This structure is tetragonal and doubly modulated on the average. The solid lines are phase solitons (or DC's); dashed lines are amplitude solitons as defined in Ref. 18.

phase are in agreement with theoretical considerations[18] if we intepret the images of the $2q$ phase as presenting periodic amplitude modulations. However, it is clear that an ideally regular DC pattern is never realized in practice. Pinning by defects is the most probable reason for this disorder, and a detailed study of the influence of defects on the IP is the subject of a separate study.[7]

ACKNOWLEDGMENTS

It is a pleasure to thank Dr. G. Errandonéa, Dr. J. Schneck, and Dr. J. C. Tolédano for many helpful discussions during this work and for a fruitful, critical reading of the manuscript. Dr. H. Mutka wises to thank the Academy of Finland for a grant for a visit to Toulouse.

---

*Present address: Institut Laue-Langevin, 156 X, 38042 Grenoble, Cedex, France.

[1]J. Schneck and F. Denoyer, Phys. Rev. B **23**, 383 (1981).

[2]J. Schneck, J. C. Tolédano, C. Joffrin, J. Aubrée, B. Joukoff, and A. Gabelotaud, Phys. Rev. B **25**, 1766 (1982).

[3]J. Schneck, Ph.D. thesis, Paris University, 1982.

[4]J. C. Tolédano, J. Schneck, and G. Errandonéa, in *Incommensurate Phases in Dielectrics,* edited by R. Blinc and A. P. Levanuyk (North-Holland, Amsterdam, 1985), Vol. II.

[5]J. M. Kiat, G. Calvarin, and J. Schneck, Jpn. J. Appl. Phys. Suppl. **24-2**, 832 (1985).

[6]C. Manolikas, J. Schneck, J. C. Tolédano, J. M. Kiat, and G. Calvarin, Phys. Rev. B **35**, 8884 (1987).

[7]S. Barré, H. Mutka, C. Roucau, A. Litzler, J. Schneck, J. C. Tolédano, S. Bouffard, and F. Rullier-Albenque (unpublished).

[8]J. Schneck *et al.* (unpublished).

[9]J. C. Tolédano (unpublished).

[10]J. P. Jamet and P. Lederer, J. Phys. Lett. (Paris) **44**, L257 (1983).

[11]J. C. Tolédano, G. Errandonéa, J. Schneck, A. Litzler, H. Savary, F. Bonnouvrier, and M. L. Estéoule, Jpn. J. Appl. Phys. Suppl. **24-2**, 290 (1985).

[12]S. Barré, H. Mutka, C. Roucau, and G. Errandonéa, Phase Transit. **9**, 225 (1987).

[13]G. Van Tendeloo, S. Amelinckx, C. Manolikas, and Wen Shuli, Phys. Status Solidi A **91**, 483 (1985).

[14]Pan Xiaoqing, Hu Mei Shen, Yao Ming-Hui, and Feng Duan, Phys. Status Solidi A **92**, 57 (1985).

[15]S. Barré, Ph.D. thesis, Paul Sabatier University, Toulouse, France, 1987.

[16]G. H. Chen, J. M. Gibson, and R. M. Fleming, Phys. Rev. B **26**, 184 (1982).

[17]K. K. Fung, S. McKernan, J. W. Steeds, and J. A. Wilson, J. Phys. **14**, 5417 (1981).

[18]J. C. Toledano and P. Tolédano, *The Landau Theory of Phase Transitions* (World-Scientific, Singapore, 1987).

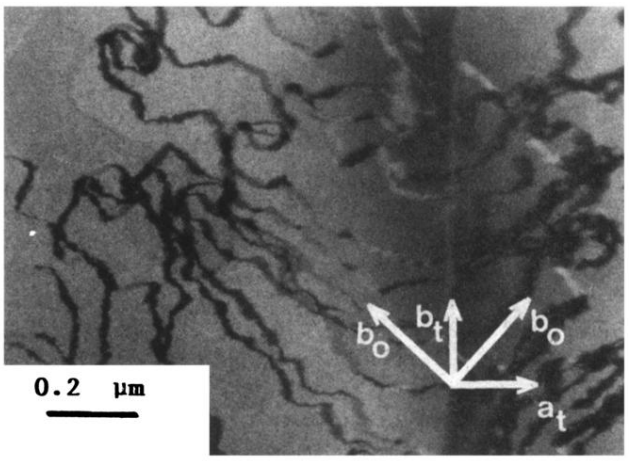

FIG. 2. Satellite dark-field micrograph obtained at RT. Two ferroelastic variants separated by a ferroelastic wall parallel to a_t or b_t are visible. In each domain, dark lines, parallel to b_0, on the average are discommensurations.

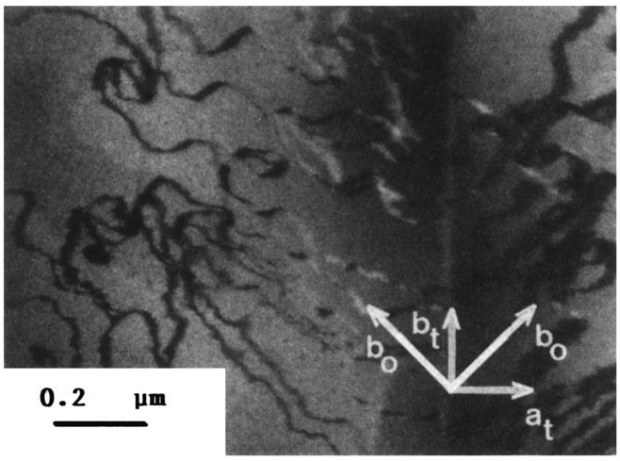

FIG. 3. Satellite dark-field micrograph obtained at RT at the end of a cycle on the same region as the one presented in Fig. 2. We observe the same pattern of DC.

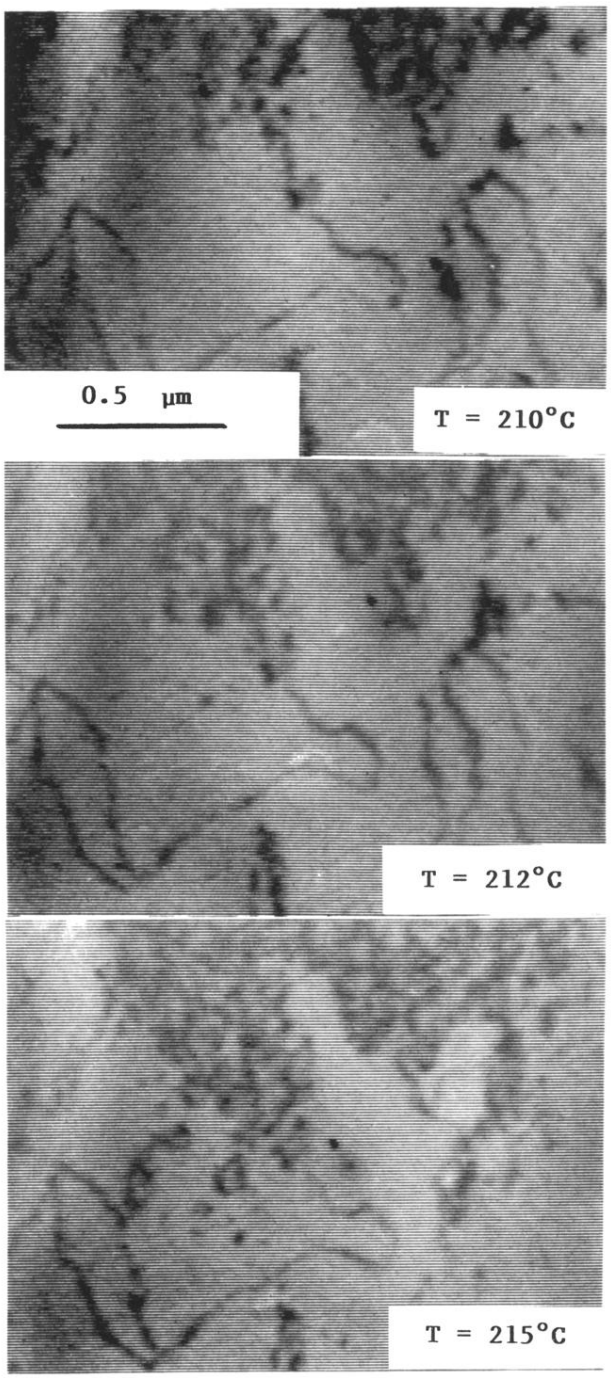

FIG. 5. This sequence shows the development of the incommensurate phase during a heating run at 2.5 °C/min. It occurs by nucleation of the discommensurations.

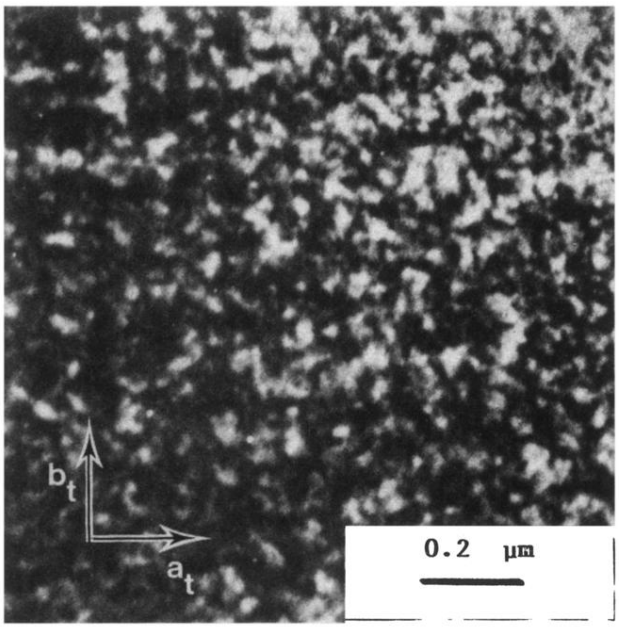

FIG. 6. Satellite dark-field micrograph of the incommensurate phase obtained at $T=230\,°C$.

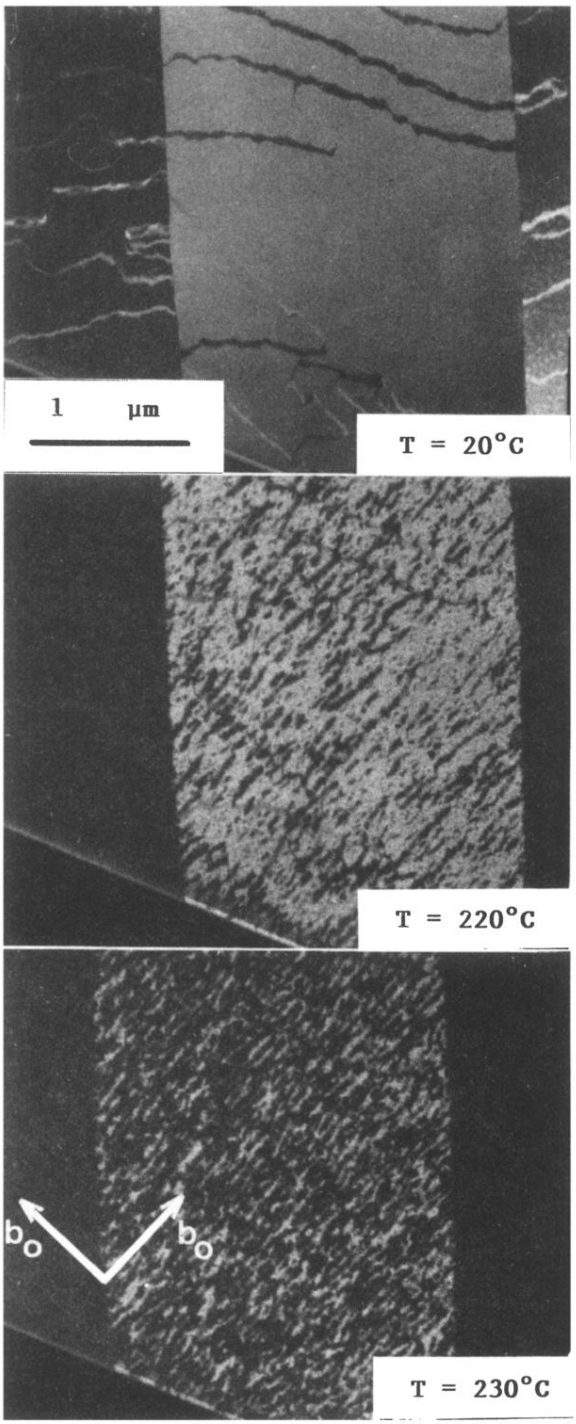

FIG. 7. Satellite dark-field micrographs obtained at different temperatures during a thermal cycle at 2.5 °C/min after annealing at $T_A = 230$ °C. We observe the nucleation of the 1q phase in the $[1\bar{1}0]_t$ priviledged direction. In the two neighboring ferroelastic domains the nucleation of the IP occurs in two perpendicular directions.

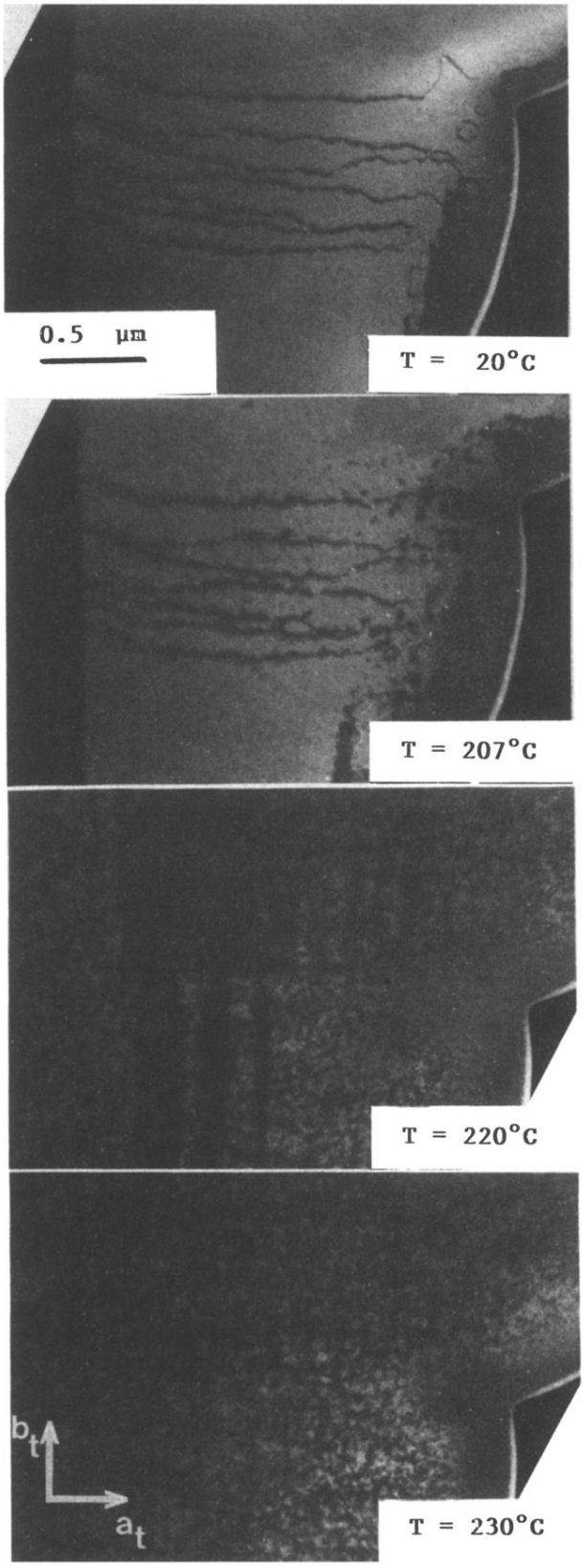

FIG. 8. Satellite dark-field micrographs obtained at different temperatures during a thermal cycle at 2.5 °C/min after annealing at $T_A = 270$ °C. We observe the nucleation of the $2q$ phase by multiplication of ferroelastic domains.